



Universiteit
Leiden
The Netherlands

Witnessing the process of bacterial cell death: novel antimicrobials and their mechanisms of action

Ouyang, X.

Citation

Ouyang, X. (2021, November 23). *Witnessing the process of bacterial cell death: novel antimicrobials and their mechanisms of action*. Retrieved from <https://hdl.handle.net/1887/3244017>

Version: Publisher's Version

License: [Licence agreement concerning inclusion of doctoral thesis in the Institutional Repository of the University of Leiden](#)

Downloaded from: <https://hdl.handle.net/1887/3244017>

Note: To cite this publication please use the final published version (if applicable).

Harzianic Acid, a Multi-Target Antimicrobial Agent Against Gram-Positive Bacteria

CHAPTER 5

Xudong Ouyang^{1,2}, Wouter A.G. Beenker¹, Jelmer Hoeksma¹,
Samantha van der Beek¹ and Jeroen den Hertog^{1,2}

1. Hubrecht Institute-KNAW and University Medical Center Utrecht,
Utrecht, the Netherlands

2. Institute Biology Leiden, Leiden University,
Leiden, the Netherlands

ABSTRACT

The thermophilic fungus *Oidiodendron flavum* is a saprobe that is commonly isolated from soil. Previously, we identified a Gram-positive bacteria-selective antimicrobial secondary metabolite (SM) from this fungal species, harzianic acid (HA). With an imaging-based mechanism of action (MoA) identification strategy, we predicted that HA targets the cell envelope. Here, we investigated the MoA of HA in more detail, using *Bacillus subtilis*. HA targeted the cell membrane, but only at high concentrations. We isolated a HA-resistant strain, M9015, and discovered that the mutant harbors five mutations in the coding region of four distinct genes. Further analysis of these genes might provide more insight into the MoA of HA at low concentrations. We conclude that HA is a multi-target antimicrobial agent against Gram-positive bacteria.

INTRODUCTION

The genus of *Oidiodendron* was established under the *Myxotrichaceae* family by Robak in 1932 [1]. Species of *Oidiodendron* are known as saprobes and are commonly isolated from a wide range of habitats, including soil, decaying plant materials, marine sediments and decomposing human hair [2–5]. They primarily occur through the temperate regions, with a few exceptions from tropical and subtropical locales. The widespread distribution of this genus is in connection with their excellent adaptive capacity, by which they establish various interactions with other organisms [6–8].

An important fungal trait for interaction with their surroundings is the production of secondary metabolites (SMs), which are not essential for fungal growth [9]. These compounds are chemically distinct small molecule compounds (in most cases < 3 kDa) often with biological activities that are produced at specific stages of growth to perform important functions, including survival from harsh environments, communication with invaders or alteration of fungal development [10]. SMs are synthesized along different pathways than primary metabolites [11] and they are excellent sources of potential therapeutic drugs [12]. Whereas the genus of *Oidiodendron* has drawn much attention with respect to studies of morphology and taxonomy [6,13], there are not many investigations into their ability to produce SMs.

Oidiodendron flavum is a thermophilic fungus and a member of the genus *Oidiodendron* [6]. Previously, we identified an antimicrobial SM from this fungal species, harzianic acid (HA). HA was first isolated as a novel antimicrobial agent from a fungal strain *Trichoderma harzianum* in 1994 [14]. Surprisingly, subsequent research focused more on the activity of HA as a plant promotor rather than an antimicrobial [11,15]. Therefore, not much data is available regarding its antimicrobial activity yet. Since HA strongly inhibits bacterial growth, it is suggested to be a promising candidate to achieve clinical application. Thus, further research into identification of its mechanism of action (MoA) is required.

Recently, we developed an imaging-based strategy, dynamic bacterial cytological profiling (DBCP), to classify antimicrobials into different classes based on their MoAs and hypothesized that HA targets the cell envelope (**Chapter 4**). Here, we applied several assays to confirm this hypothesis and to unravel further details about its MoA. In addition, we isolated HA-resistant bacteria and identified four mutated genes, which provides further insight into its MoA.

MATERIALS AND METHODS

Strains and reagents

B. subtilis strain 168 was used for MoA identification in this study [16]. *O. flavum* (CBS 366.71) was obtained from the Westerdijk Fungal Biodiversity Institute (the Netherlands) and used for biologically active compound production. Pathogenic bacterial strains used for activity tests were either obtained from ATCC or they were clinical isolates (kind gift from University Medical Center Utrecht, the Netherlands) and they are listed in Table S1. Commercial antimicrobials and resazurin were purchased from Sigma Aldrich. FM4-64, DiSC₃(5) and SYTOX-Green were purchased from Thermo Fisher Scientific.

Microdilution assay

Minimum Inhibitory Concentration (MIC) was determined by broth microdilution assay as previously described [17]. The freshly prepared early exponential-phase cell cultures of different strains were diluted 1 : 100 into Luria-Bertani (LB) medium, and then distributed in a 96-wells plate. Antimicrobials were tested starting at a 10 × dilution of the stock in DMSO, which was then serially diluted with a factor 2. MIC was defined as the lowest dilution at which bacteria did not grow, based on visual inspection after an overnight incubation at 37 °C.

Growth curves

Overnight bacterial cultures of *B. subtilis* were diluted 1 : 50 into fresh LB medium and incubated at 37 °C with shaking. For the accurate MIC of HA determination, OD₆₀₀ of cultures were measured by a FLUOstar microplate reader (BMG Labtech) every 30 min for 24 h. At an early exponential-phase of cultures with an OD₆₀₀ of 0.3, different concentrations of HA were added. For the comparison of *B. subtilis* strain 168 and M9015, OD₆₀₀ of both cultures was measured using a Bioscreen C Microbiology Reader every 15 min for 24 h.

Confocal microscopy

Microscopy was performed following the protocol described before with minor modification [18]. Briefly, samples were immobilized on microscope slides covered with an agarose pad containing 1% agarose and LB medium, and imaged. Confocal microscopy was carried out using a Perkin Elmer UltraView VoX spinning disk

microscope system, consisting of a Leica DMI6000 microscope equipped with a 100 × NA1.47 oil objective, a Yokogawa X1 spinning disk unit, a Hamamatsu Orca Flash4.0 V3 camera, and Volocity v6.3 software. Z-stack images were collected over a length of 3 μm with 0.2 μm intervals to acquire signals from the whole cells. Experiments were done with biological triplicates. Images were analyzed using Fiji [19].

Sporulation inhibition assay

This assay was applied as previously described with modifications [20]. The freshly prepared early exponential-phase cell cultures of *B. subtilis* with an OD₆₀₀ of 0.3 in LB media were centrifuged and resuspended in 1/10 of the original volume. Antimicrobials (5 × MIC) or DMSO (control) were added and 15 μL of the mixtures were transferred into 1.5 mL tubes to incubate with rolling at 37 °C for 5 h. Cells were then stained with FM 4–64, immobilized and imaged.

Cytotoxicity assay

For the cytotoxicity assay, HepG2 cells were seeded in 96-well plates and grown in DMEM low glucose medium (ThermoFisher, 10567014) supplemented with 10% FBS. Test compounds were added in different concentrations, with a final concentration of 1% DMSO and cells were incubated for 20 h at 37 °C with 5% CO₂. Next, resazurin was added to reach a final concentration of 0.1 mM. After 3 h incubation, the fluorescence was measured on a PHERAstar microplate reader (BMG Labtech) using an excitation wavelength of 540 nm and emission wavelength of 590 nm. The average intensity of DMSO control was set as 100% alive and the percentage of intensity from each treated sample was calculated. IC₅₀ was calculated using nonlinear regression in GraphPad Prism. Experiments were conducted in biological triplicates.

Resazurin assay

This assay was applied as previously described with modifications [18]. Resazurin is an oxidation–reduction indicator (excitation at 530–570 nm, emission at 580–590 nm) [21]. Freshly prepared early exponential-phase *B. subtilis* cultures with an OD₆₀₀ of 0.3 in LB medium were treated with antimicrobials (5 × MIC) or DMSO (control) for 5, 30 and 60 min. Untreated cells and boiled cells (95°C for 10 min) were used to calculate the standard respiration and no respiration, respectively. Next, cells were washed with medium by centrifugation and afterwards resuspended in medium to adjust the OD₆₀₀ to 0.15. Cells were then incubated with 30 μg/mL resazurin for 45

min at 37 °C. Absorbance of different samples was measured using a 540 nm/590 nm filter.

Cell depolarization assay and cell permeability assay

DiSC₃(5) is commonly applied for cell depolarization assay because it generally accumulates in well-energized cells. Disruption of membrane potential releases this probe from cells into the medium, resulting in an increase of overall fluorescence in the cell suspension [22]. SYTOX green was used in the cell permeability assay. This dye is cell impermeable and its fluorescence signal increases significantly when bound to DNA [23]. To perform these assays, the freshly prepared early exponential-phase cell cultures with an OD₆₀₀ of 0.3 in LB medium were stained with DiSC₃(5) or SYTOX green for 10 min. Then the fluorescence was measured on a PHERAstar microplate reader (BMG Labtech) using a 540 nm/590 nm filter for DiSC₃(5), or a 485 nm/520 nm filter for SYTOX green. Experiments were conducted in biological triplicates.

Lipid assay

This assay was applied as previously described with modifications [24]. The appropriate amounts of antagonists lipid I, lipid II and C₅₅-P in CHCl₃ : MeOH (1 : 1) were added to the 96-well plates and the solvent was evaporated. The antagonists were re-dissolved in LB containing antimicrobials (2 × and/or 1 × MIC) or 1% DMSO in solution. The freshly prepared early exponential-phase cell cultures of *B. subtilis* were diluted 1 : 100 into LB medium, and then distributed in the 96-wells plate with antagonists and antimicrobials. After incubation overnight at 37 °C, bacterial growth was inspected visually.

Screening for HA-resistant mutants

To obtain HA-resistant mutants, we grew *B. subtilis* in the presence of 1 x MIC of HA in LB medium at 37 °C with shaking. Once bacterial growth was observed, it was sequentially transferred to medium with 2-fold higher concentrations of HA. The whole process was set for a period of 28 days.

Scanning electron microscopy

Overnight cultures of *B. subtilis* strain 168 and M9015 were transferred to fresh LB medium and grown to mid-log phase. Bacterial cells were then washed, fixed,

dehydrated, mounted onto 12.5 mm specimen stubs and coated with gold to 1 nm as previously described [25]. Samples were imaged using a Phenom PRO desktop SEM (Phenom-World BV). Cell width was measured from 10 cells for each strain from triplicate images using Fiji.

Peptidoglycan analysis

This assay was performed following a previous protocol [26]. The overnight bacterial culture of *B. subtilis* was diluted 1 : 50 into 400 mL fresh LB medium and incubated at 37 °C with shaking until reaching expected cell density. The cell culture was then chilled on ice and centrifuged at 5,000 x g for 10 min at 4 °C. After washing twice with cold PBS, the cell pellet was resuspended in 10 mL PB (25 mM sodium phosphate, pH 6.0), disrupted using beads beater, mixed with 10 mL of 10% (w/v) SDS in a boiling water bath, boiled for 30 min and incubated at 37 °C overnight. Next, the sample was centrifuged at 45,000 x g for 30 min at 20 °C to pellet the insoluble peptidoglycan, which was then washed with 10 mL of PB 4-6 times, suspended in 2 mL PB and transferred to a microcentrifuge tube. After adding 200 µg/mL of pronase and incubating for 2 h at 37 °C with agitation, TCA hydrolysis was performed at 4 °C for 18 h with constant shaking. Afterwards, the hydrolyzed sample was centrifuged at 45,000 x g for 30 min at 20 °C to pellet the insoluble peptidoglycan, which was then washed three times, suspended in 5 mL PB. After digestion of peptidoglycan using 0.5 mg/mL lysozyme overnight and reduction of sugars using sodium borohydride for 20 min, sample was ready for HPLC analysis, which was performed using a Shimadzu LC-2030 system with PDA detection (190-800 nm) and a Shimadzu Shim-pack GISTC18-HP reversed phase column (3 µm, 4.6 × 100 mm). The mobile phase was 50 mM sodium phosphate pH = 4.33 (buffer A) and 50 mM sodium phosphate pH = 5.1 with 15% (v/v) methanol (buffer B). A flow rate of 0.5 mL/min was applied using the following protocol: buffer A for 10 minutes followed by a linear gradient of buffer B (0–100%) for 120 minutes, 100% buffer B for 10 minutes, another linear gradient of buffer B (100–0%) for 5 minutes and finally buffer A for 5 minutes.

Genomic DNA sequencing

The bacterial cell wall of *B. subtilis* was lysed using 0.5 mg/mL lysozyme for 1 h at 37 °C. Next, genomic DNA was isolated using the Wizard Genomic DNA purification Kit (Promega) and sequenced by Illumina Next Generation Sequencing in University Medical Center Utrecht.

Bioinformatic analysis

The raw sequencing reads were subjected to a panel of bioinformatic analyses including quality control using FastQC and Trimmomatic, alignment to reference genome using BWA-MEM algorithm and variant calling using Integrative Genomics Viewer (IGV). The published genome sequence of *Bacillus subtilis* subsp. *subtilis* str. 168 was used as the reference genome, which has a NCBI accession number of NC_000964.3.

RESULTS

HA is a selective antimicrobial against Gram-positive bacteria

HA was tested against a panel of 14 pathogenic bacteria, including seven Gram-positive and seven Gram-negative strains (Table S1). The growth of all Gram-positive bacteria was affected with Minimum Inhibitory Concentrations (MICs) ranging from 25 to 200 µg/mL. The panel included antibiotic-resistant pathogenic bacteria, which were sensitive to HA, e.g. methicillin resistant *Staphylococcus aureus* (MRSA) at 200 µg/mL and vancomycin resistant *Enterococcus faecium* (VRE) at 100 µg/mL. No inhibition was observed in response to HA of any of the Gram-negative bacteria tested up to 400 µg/mL. This indicates that HA is a selective antimicrobial agent against Gram-positive bacteria. Next, to assess the toxicity of this compound on human cells, cytotoxicity assays were done using the HepG2 cell line, originating from human liver. The IC₅₀ for HA was 226.6 µg/mL (Fig. 1A), indicating that human cells have a higher tolerance for HA than Gram-positive bacterial cells.

HA induced lysis of Bacillus subtilis cells

To further explore the antimicrobial properties of HA against Gram-positive bacteria, a model Gram-positive organism, *B. subtilis* strain 168, was used for the following assays. First, to obtain an accurate MIC, the growth curves of *B. subtilis* were measured in the presence of a range of HA concentrations (Fig. 1B). Although cells were also affected at concentrations of 30 and 40 µg/mL, total inhibition of cell growth after 18 h (overnight) was only seen at a concentration of 50 µg/mL and higher, suggesting that the correct MIC for *B. subtilis* was 50 µg/mL. In the following assays, we used 250 µg/mL (5 × MIC) HA to ensure the effects on cells, unless specified differently. Interestingly, a decrease in OD₆₀₀ was observed 30 min after addition of the compound with all concentrations of HA, even with the lowest

concentration, 30 $\mu\text{g}/\text{mL}$. This decrease was not observed with vehicle control (DMSO), indicating that this decrease was not an artefact. These results suggest that HA induced cell lysis soon after addition to the cells. Some microorganisms, including *B. subtilis*, respond to harsh environments by entering a robust resting state, the endospore, which is self-protective. During that process, cells may also lyse [27]. To determine whether HA destroyed the cells and/or induced the cells to form endospores, a sporulation assay was performed. In the control-treated cultures (Fig. 1C), spores were generated by some of the cells during high-density culturing overnight. However, following overnight HA treatment, no intact cells were observed and no clear spores were observed either (Fig. 1D). These results suggest that HA destroyed the cells without inducing spore formation.

Pore formation is the initial effect of HA on bacterial cells

Using DBCP, we previously predicted that HA generated pores on the bacterial cell membrane and inhibited cell growth immediately after addition to cells (**Chapter 4**). To confirm this mechanism, we first investigated bacterial cell viability using a resazurin assay [21]. Our results (Fig. 1E) showed that after 5 min treatment, 99% of cells lost their viability. None of the cells seemed to be viable after HA treatment for 60 min. This confirms that HA has an immediate effect when added to bacteria.

Next, we used $\text{DiSC}_3(5)$ to detect changes in transmembrane potential [22]. Carbonyl cyanide *m*-chlorophenyl hydrazone (CCCP) and nisin were selected as positive controls, because they are known to destroy the membrane potential by disruption of cellular ionic homeostasis and generation of pores in the cell membrane, respectively [28,29]. Similar to treatment with CCCP or nisin, HA induced a sudden increase of fluorescence in cells (Fig. 1F), suggesting that disruption of the membrane potential was an immediate effect.

To determine whether the loss of membrane potential was due to a pore-forming activity or not, cell permeability was investigated with SYTOX green [23]. As shown in Fig. 1G, the fluorescence intensity of the cell suspension gradually increased upon HA and nisin treatment, but not CCCP treatment. This suggests that the disruption of membrane potential in response to HA was caused by pore formation.

Vancomycin- and nisin-induced cell lysis is caused by binding to lipid II [29,30]. To determine if HA-induced pore formation was also mediated by binding to lipid II in the membrane, lipids were added to the bacterial cultures prior to addition of HA. If HA binds directly to lipid II or precursors, the externally added lipids will quench HA and hence, addition of HA will not affect bacterial growth [24]. Several

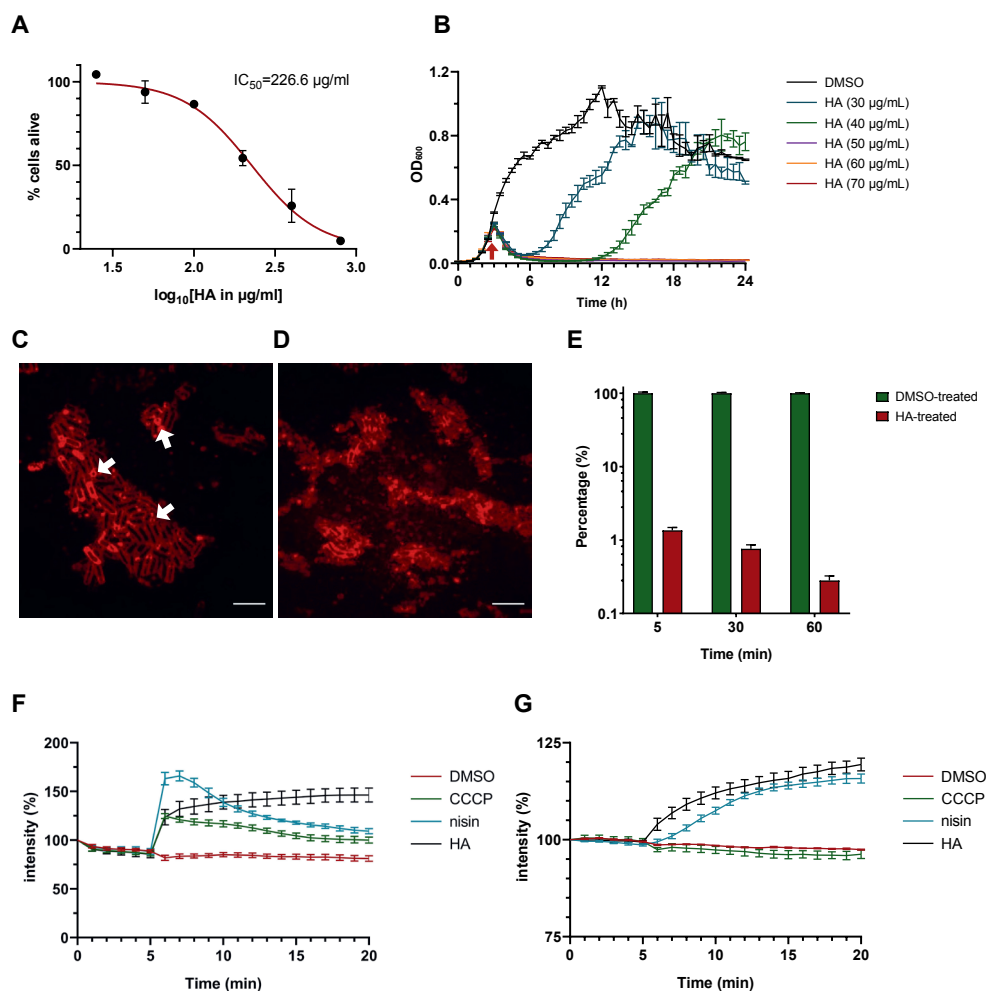


Fig. 1. Antimicrobial property of HA. (A, B) HA inhibits eukaryotic cell growth and bacterial growth. (A) Cytotoxicity assay. HepG2 cells were incubated with HA in different concentrations for 20 h before addition of resazurin. The ability to reduce blue resazurin to red resorufin was measured at 540 nm. The average intensity of DMSO control was set as 100% alive and the percentage of intensity from each treated sample was calculated. The mean from biological triplicates was plotted with error bars representing the SEM in black. Nonlinear regression was analyzed and plotted in red, on which IC₅₀ was based. (B) Growth curves of *B. subtilis* strain 168/WT in the presence of a range of HA concentrations. OD₆₀₀ was measured every 30 min. HA was added at 2.5 h (arrow). The graph depicts the average and the SEM of biological triplicates. (C, D) No sporulation in response to HA. *B. subtilis* cells from a high density overnight culture were treated with (C) DMSO (control) or (D) HA (250 $\mu\text{g ml}^{-1}$, 5 \times MIC), stained with FM4-64 and imaged by confocal fluorescence microscopy. Representative images are shown. Example spores in the DMSO

control are indicated with arrows. Scale bar is 5 μm . (E) HA rapidly blocks respiratory chain activity in *B. subtilis*. Effect on respiratory chain activity measured by the reduction from blue resazurin to red resorufin at 540 nm. The average intensity of DMSO control in each group was set to 100% intensity. HA (250 $\mu\text{g ml}^{-1}$, 5 \times MIC) was added and after 5, 30 and 60 min, the percentage of conversion was calculated relative to the control. The mean from biological triplicates was plotted with error bars representing the SEM. The log 10 format was used for the scale of the Y axis. (F, G) HA treatment induced membrane permeability. (F) Membrane potential measurement. *B. subtilis* membrane potential levels were quantified using the fluorescent dye DiSC₃(5). CCCP (2 $\mu\text{g ml}^{-1}$, 5 \times MIC), nisin (12.5 $\mu\text{g ml}^{-1}$, 5 \times MIC) or HA (250 $\mu\text{g ml}^{-1}$, 5 \times MIC) (as indicated) or DMSO was added after 5 min. The fluorescence was depicted as percentage of the value at the start (t = 0 min) (y-axis) over time (x-axis, min). The mean from biological triplicates was plotted with error bars representing the SEM. (G) Membrane permeability measurement. Experiments were performed as in (F), except for using a different dye SYTOX-Green for quantifying membrane permeability.

lipid II precursors were selected: C55P, lipid I and lipid II. Vancomycin (0.5 $\mu\text{g/mL}$, 2 \times MIC) and nisin (5 $\mu\text{g/mL}$, 2 \times MIC) were used as positive controls for this assay. *B. subtilis* cells were treated with these control antimicrobials in the presence or absence of 10 μM of the different lipids and bacterial cell growth was determined (Table S2). The antimicrobial effects of nisin and vancomycin were quenched by exogenous lipid I and lipid II as expected. C55P also affected antimicrobial activity of nisin. For HA, both 2 \times MIC (100 $\mu\text{g/mL}$) and 1 \times MIC (50 $\mu\text{g/mL}$) were tested in the presence of 10 μM or even 150 μM of the different lipids. However, the activity of HA was not affected by addition of any of these lipids, suggesting the mechanism underlying pore formation by HA and nisin are distinct.

Screening for HA-resistant mutants

Knowledge about antimicrobial resistance may provide insight into the underlying MoA. Inducing resistance by prolonged exposure to increasing concentrations of antimicrobial agents is a proven method. To obtain insight into the MoA of HA, we grew *B. subtilis* in the presence of 1 \times MIC of HA for three days. Under these conditions, three colonies grew and these were transferred sequentially to medium with 2-fold higher concentrations of HA. Over a period of 28 days, one colony was successfully grown in medium with 4 \times MIC of HA. Resistance against an antimicrobial may be due to either gene mutation or gene expression adaptation. To

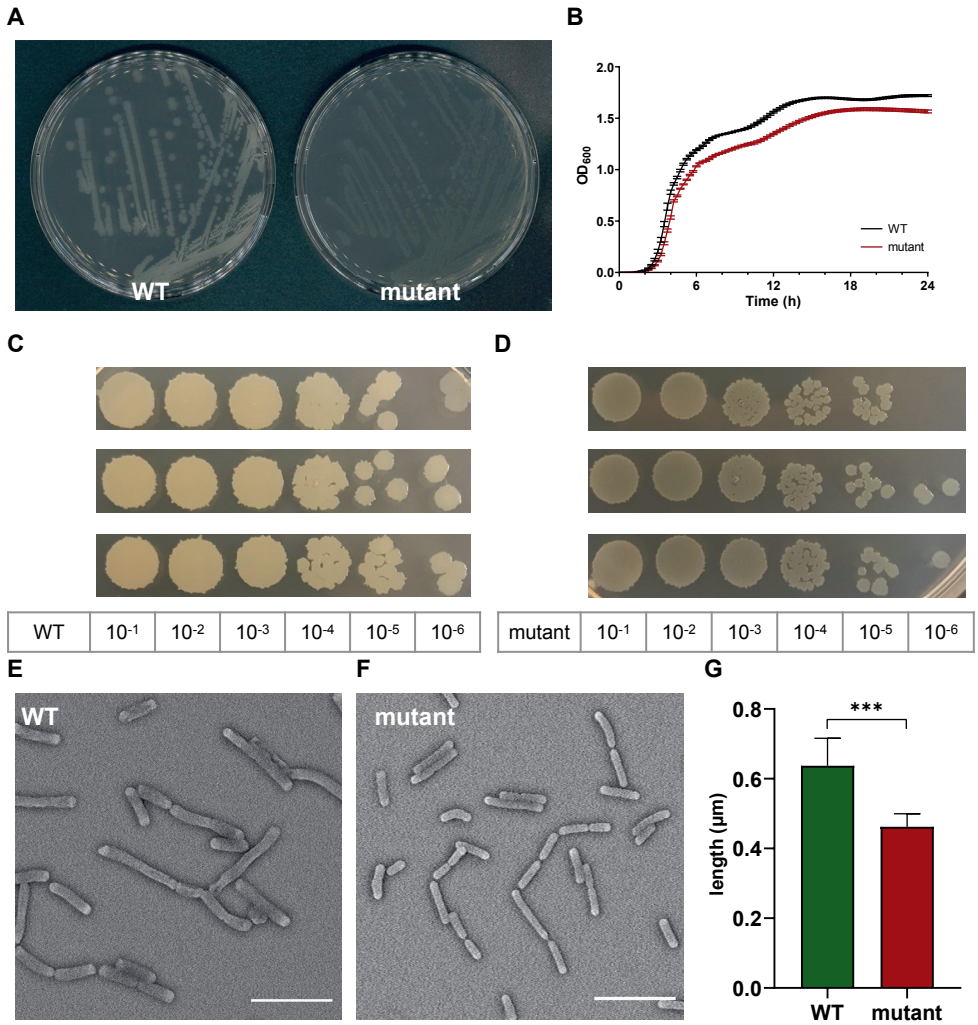


Fig. 2. HA-resistant M9015 colonies are translucent and mutant cells are smaller. (A) *B. subtilis* strain 168/WT and M9015 plated on LB agar. (B) Growth curves of WT and M9015. OD₆₀₀ was measured and the mean from biological triplicates was plotted with error bars representing the SEM. (C and D) CFU counting. The overnight cultures (18 h) of WT and M9015 were serially diluted, and 5 μL of each diluted sample was dropped on LB agar. Experiments were performed with biological triplicates. (E and F) The cells from overnight cultures (18 h) of WT and M9015 were fixed and imaged by scanning electron microscopy. Representative images are shown. The width of cells was measured and plotted in (G); mean with error bars representing the SEM is depicted; *** indicates $p \leq 0.001$ by student t-test.

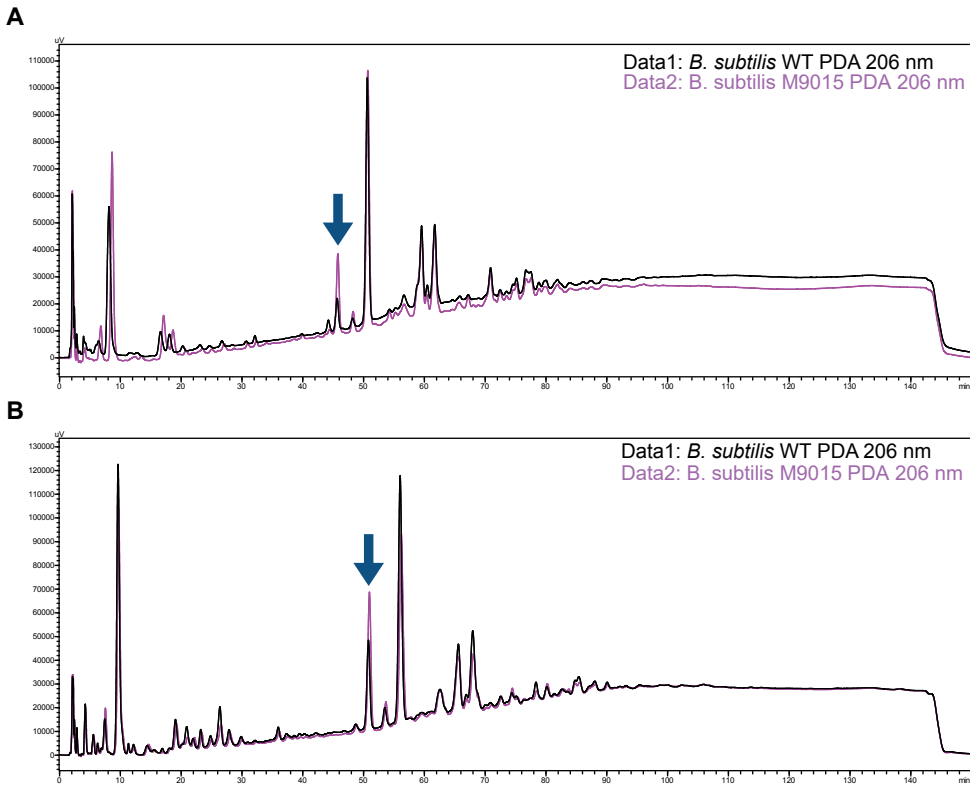


Fig. 3. Similar peptidoglycan pattern between *B. subtilis* strain 168 and M9015. Peptidoglycan of both strains from overnight culture (A) and exponential phase culture (B) were isolated, digested and analyzed by analytical HPLC. The arrow in each figure indicated the peak that differed most between the two strains.

distinguish between these possibilities, we cultured the resistant bacteria without HA for ten serial passages. Finally, an accurate microdilution assay showed that this strain, dubbed *B. subtilis* strain M9015, had a maximum tolerance of 250 $\mu\text{g}/\text{mL}$, which is 5 \times higher than the MIC of wild type *B. subtilis* strain 168. HA resistance persisted in the M9015 strain, suggesting that resistance is caused by mutations in the genome.

The M9015 strain was not only resistant to HA, but the colonies also had a different appearance on agar plates than wild type. *B. subtilis* strain M9015 colonies had a more translucent appearance, but the colony size did not differ much between the wild type and M9015 strains (Fig. 2A). We assumed that this interesting phenotype

might be due to a slower growth rate (i.e. less cells), smaller cell size or a structural change in the cell wall (i.e. cells were more translucent). To investigate this, the growth curves of the strains were first compared. The growth pattern of both strains was similar, but the mutant had a 15 min longer period in the lag phase and a 0.2 lower final optical density at 600 nm in the stationary phase (Fig. 2B). Next, the number of cells in the overnight culture was determined (Fig. 2C, D). The cell density in the mutant strain was 2.2×10^8 CFU/mL, which was 57% higher than wild type (1.4×10^8 CFU/mL). Comparison of the cell size using a scanning electron microscope (Fig. 2E, F) showed that M9015 mutant cells were 27 ± 5 % smaller than wild type cells (Fig. 2G). These results suggest that the cell size affected the appearance of M9015 colonies.

To determine if there were changes in the structure of the cell wall that also contributed to the translucent phenotype, we analyzed the peptidoglycans. To this end, the cell wall was isolated from overnight cultures of both strains, followed by lysozyme digestion and HPLC analysis. Almost all peaks were matching between the M9015 mutant and wild type (Fig. 3A). However, one peak (arrow indicated) in the mutant sample was higher than in wild type. Peptidoglycan analysis of exponential phase cultures of these two strains showed similar results (Fig. 3B). It is unlikely that

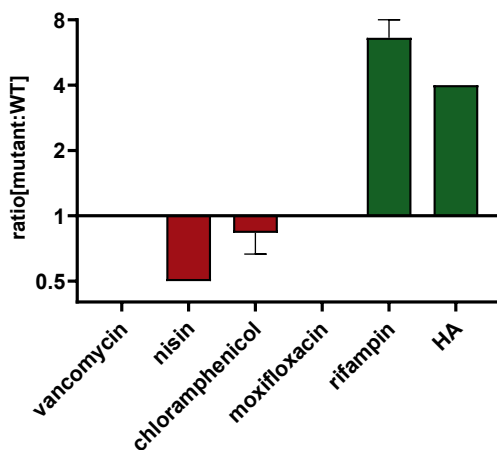


Fig. 4. HA-resistant M9015 strain is also resistant to rifampin. MICs of selected antimicrobials against WT or M9015 were measured. The ratio of the MIC of a certain antimicrobial against M9015 to that against WT was calculated. The mean of the ratio from biological triplicates was plotted with error bars representing the SEM. The red bars indicated that M9015 was more sensitive to certain antimicrobial whereas the green bars indicated the opposite. The log 2 format was used for the scale of Y axis.

the slight difference in peptidoglycan composition of the cell wall contributed to the different appearance of the M9015 strain. However, this remains to be determined definitively.

Cross resistance of the M9015 strain to other antimicrobials might provide valuable insight into the resistance class of this mutant strain. Therefore, we compared the MICs on M9015 mutant and wild type strains of antimicrobials from five major classes: nisin, vancomycin, chloramphenicol, moxifloxacin and rifampin. Interestingly, M9015 showed reduced sensitivity to rifampin, an RNA class antimicrobial, to a similar extent as HA (i.e. 4- to 8-fold; Fig. 4). No significant differences were observed for any of the other antimicrobials, which included antimicrobials targeting the cell envelope. It is surprising that the HA-resistant M9015 strain is also more resistant to the RNA class antimicrobial rifampin, because our earlier DBCP experiments suggested that HA targets the cell envelope.

Identification of mutations in M9015 by genomic sequencing

In order to determine which pathway(s) was/were affected in M9015, the genomes of M9015 mutant and wild type strains were sequenced by Next Generation Sequencing. The published genome sequence of *Bacillus subtilis* subsp. *subtilis* str. 168 was used as the reference genome. The mapping of the reads from our wild type strain against this referenced genome showed high coverage (only around 2,000 mutation sites), suggesting this reference is applicable, which facilitated the alignment of our sequencing data. Bioinformatic comparison of the wild type and mutant genomes resulted in the identification of ten potential variations (Table S3), five of which were suggested to be reliable by the Integrative Genomics Viewer (Fig. S1, S2). These five mutations were located in the coding region of four different genes, *ymaB*, *flgL*, *atpE* and *yusO* (twice).

The mutations in *ymaB* and *atpE* were single-base substitutions causing an amino acid substitution in their protein products. YmaB is a putative Nudix hydrolase with RNA pyrophosphohydrolase activity [31], and the mutation we found resulted in a p.L138P substitution (Fig. 5A). Although both these amino acids are non-polar and hydrophobic, their structures differ substantially, which might affect the activity of YmaB. The function of this gene is not clearly described in literature yet, and therefore the effect of the observed mutation remains unclear. The *atpE* gene encodes the subunit c of ATP synthase [32]. In M9015, we identified a p.A51V substitution (Fig. 5B). The property of these two amino acids is quite similar, but the larger size of Val in the mutant might affect the activity of AtpE severely.



Fig. 5. Mutated genes of M9015. The genes of *ymaB* (A), *atpE* (B), *yusO* (C) and *flgL* (D) are shown. Each gene was presented with DNA sequence (grey line with numbers indicating the length of DNA) and protein sequence (green line with green blocks indicating the sites of initiation codon). Red blocks in the mutated gene and protein sequences indicate the mutated sites.

The *yusO* gene expresses YusO, a transcription repressor, which binds to the *yusOP* promoter region and thus represses *yusOP* expression. YusP confers low-level resistance to fusidic acid, novobiocin, streptomycin, and actinomycin [33]. This gene was disrupted by two insertions in M9015 mutant cells: a single-base insertion (c.199_200insA), introducing a frame shift and stop-codon and an in-frame nine-base insertion (c.454_455insGAGGAAACG). Therefore, the gene product would be different from the wild type strain (Fig. 5C). Instead of expressing YusO, the M9015 mutant might produce two (non-functional) truncated proteins from this gene, dubbed YusO-m1 and YusO-m2. In YusO-m1, the frame shift would result in a premature stop p.A67D fsX10. There is an alternate initiation site just past the

single base pair insertion in *yusO*, which might initiate the expression of YusO-m2. The nine base pair insertion near the 3' end of *yusO* would lead to a three amino acids duplication near the C-terminus of YusO-m2 (p.G153_G155dup). However, whether YusO-m1 and/or YusO-m2 proteins are stably expressed in M9015 remains to be determined. Hence, it is not unlikely that mutation of *yusO* might contribute to HA resistance. However, it has been reported that mutation of YusO did not confer resistance to rifampin [33], which is not in line with our results that M9015 is resistant to rifampin. This suggests that the other mutations in M9015 might also contribute to its resistance.

The *flgL* gene expresses FlgL, a flagellar hook-filament junction protein, which has a function in motility and chemotaxis [34]. It had a one base pair deletion in M9015 cells, resulting in a truncated FlgL protein (p.K35SfsX9, FlgL-m1, Fig. 5D). Potentially, a second FlgL protein, FlgL-m2 starting from Met47 of FlgL was produced in M9015 cells as well (Fig. 5D). It has been suggested that disruption of this gene may lead to reduced motility, which might contribute to the translucent appearance of M9015 colonies as well.

HA may have multiple targets and only generate pores on the membrane at high concentration

Interestingly, none of the mutated genes we identified are involved in the pathways of cell membrane synthesis or cell wall synthesis. Instead, slow-growth (*atpE*),

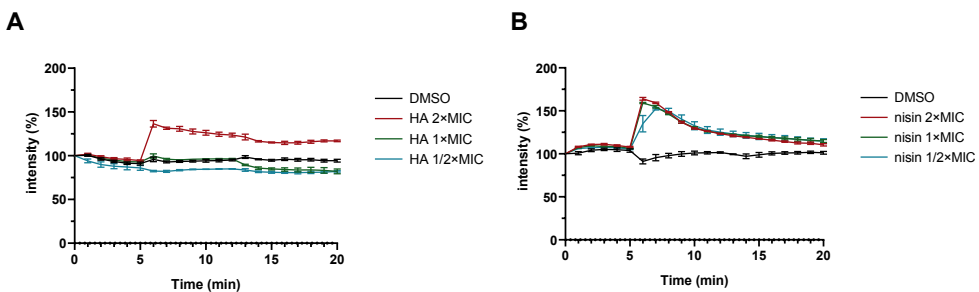


Fig. 6. HA affects cell depolarization only at high concentration. *B. subtilis* membrane potential levels were quantified as in Figure 1F and G. Different concentrations of HA (A) or nisin (B) were added after 5 min. DMSO was used as control. The fluorescence was depicted as percentage of the value at the start ($t = 0$ min) (y-axis) over time (x-axis, min). The mean from biological triplicates was plotted with error bars representing the SEM.

slow-movement (*flgL*), pumping out antimicrobials (*yusO*) and RNA hydrolysis issues (*ymaB*) may individually or collectively lead to HA resistance. Nevertheless, we observed effects of HA on the cell envelope (Fig. 1F, G). We hypothesized that HA might have multiple targets including a target in the membrane. This effect is in a way reminiscent of triclosan, which is a multi-target antimicrobial that has specific targets in the membrane only at high concentrations [35]. To investigate this hypothesis, we performed depolarization assays with different concentrations of HA. The results showed that HA did not affect cell membrane at $0.5 \times \text{MIC}$ or $1 \times \text{MIC}$ (Fig. 6A). Only at $2 \times \text{MIC}$ of HA, effects on the cell membrane were observed. Nisin treatment on the other hand showed effects on membrane polarization at all concentrations tested, even at $0.5 \times \text{MIC}$ (Fig. 6B). These results suggest that HA is a multi-target antimicrobial and that the cell membrane was targeted at higher concentrations of HA.

DISCUSSION

Here, we describe the antimicrobial property of HA. The minimum concentration of HA to inhibit *B. subtilis* growth overnight was $50 \mu\text{g/mL}$, which was around 4 to 5 times less than the IC_{50} of human cells (Fig. 1A, B). This suggested HA not to be very toxic. Treatment of bacteria with HA at concentrations below $50 \mu\text{g/mL}$ led to rapid arrest of bacterial growth and even lysis of the cells (a reduction in OD_{600}). Interestingly, following treatment with 30 or $40 \mu\text{g/mL}$ HA, bacterial growth recovered 3 to 9 hours after the start of treatment, respectively (Fig. 1B). The mechanism underlying recovery of the bacterial growth following treatment with HA below $50 \mu\text{g/mL}$ remains to be determined. The cells showed delayed but similar growth kinetics to control samples. HA may be degraded by the few live cells, or HA may be exhausted or quenched by the bacterial cells. The remaining live cells appear not to be affected by the previous presence of HA in the medium and are now able to grow freely again at the same growth rate as untreated cells.

HA was suggested to be a multi-target antimicrobial agent that generates pores in the cell membrane at high concentrations. Some antimicrobials affect membrane integrity without direct targeting of the membrane. For instance, gentamycin exclusively targets ribosomes, which results in misfolded membrane proteins. Eventually, this will lead to membrane defects [36,37]. However, the pore formation by HA is unlikely caused by such indirect mechanisms, because higher concentrations (i.e. $2 \times \text{MIC}$) of HA induced cell depolarization immediately after the addition of this compound (Fig. 1F, 6A). Since HA did not bind to any of the

provided lipids in our study (Table S2), the mechanism of the pore formation is still unclear. To further study the mechanism, other approaches, e.g. molecular dynamics simulations to model pore formation in lipid bilayers [38,39], might provide insight into the underlying mechanism.

To further study the MoA of HA, we selected a low-level HA-resistant strain, *B. subtilis* strain M9015, by continuous exposure to HA. The colonies of the M9015 mutant were more translucent than the wild type. We examined this phenotype in relation to HA-resistance. In the comparison of the growth patterns and cell size between mutant and wild type, we found that the size of M9015 cells was smaller. Smaller cell size might contribute to the translucent appearance of colonies, because the colonies will be thinner when the cells are smaller. The observed apparent reduction in growth might also be caused by reduced cell size, because the same number of bacterial cells will have a lower OD₆₀₀ when the cells are smaller. Comparison of the components of cell wall by peptidoglycan analysis indicated that there was only one peak with a subtle difference between WT and mutant (arrow in Fig. 3). However, the connection between the difference in cell wall, the smaller cell size and HA-resistance remains to be determined.

Finally, we sequenced the genomes of the M9015 mutant and wild type cells, resulting in the discovery of four mutated genes. None of these genes has a direct effect on the cell envelope. However, this may give an indication of the targets of HA at lower concentrations. The mutations of *flgL* and *atpE* seem to contribute to reduced cell mobility and cell size, respectively, which may contribute to a reduced growth rate. It is noteworthy that it was reported previously that slow growth actually conferred non-heritable antibiotic resistance in *Salmonella enterica* [40]. The mutation of *yusO* may confer resistance to some extent, because *yusO* has been implicated in antimicrobial resistance before [33]. Yet, it has been reported that *yusO* is not involved in rifampin resistance [33], whereas we found that the HA-resistant strain M9015 had cross resistance to rifampin. Therefore, it is more likely that other mutation(s) contribute(s) to HA resistance. The fourth gene that was found to be mutated in M9015 cells was *ymaB*, which might also be involved in the resistance. The *ymaB* gene is involved in RNA metabolism [31], and mutation of this gene might contribute to the observed rifampin-resistance of M9015 cells. Further study of these four genes for instance by targeted inactivation of each gene separately and/or in combinations may provide more insight into the role of these genes in antimicrobial resistance. Alternatively, it would be interesting to rescue these genes in the mutant individually and exclude the genes that do not contribute to antimicrobial resistance. We have attempted to rescue the mutated genes in the M9015 strain several times

but the cloning failed. This might be due to the gene *flgL*, which was reported to be a component of ComK regulon [41]. ComK is the competence master regulator of *B. subtilis* [42], and defective ComK function might affect the ability to make these bacteria competent. Hence, the alternate approach to inactivate each of the four genes individually and/ or in combination might help to further unravel the mechanism of action of HA.

To conclude, our results suggest HA to be a multi-target antimicrobial agent against Gram-positive bacteria. It targeted the cell membrane, but only at high concentrations. We have developed a HA-resistant strain, M9015, and discovered that mutant colonies had a more translucent appearance than wild type, which may be due to reduced cell size. The M9015 strain showed cross resistance to rifampin. However, it remains to be determined whether HA also belongs to the RNA class of antimicrobials. M9015 harbors five mutations in the coding region of four distinct genes. Further analysis of these genes might provide more insight into the MoA of HA at low concentrations.

ACKNOWLEDGEMENTS

The authors would like to thank Anko de Graaff of the Hubrecht Imaging Centre for help with imaging, Ad Fluit of the Medical Microbiology department of UMC Utrecht for clinical bacterial isolates, Eefjan Breukink (Utrecht University) for Lipid II and derivatives, Ronnie Lubbers for critical reading of the manuscript and Marieke Kuijk for help with antimicrobial activity test. This project was supported by the Chinese Scholarship Council (CSC).

REFERENCES

- [1] Robak H. Investigations regarding fungi on Norwegian ground wood pulp and fungal infection at wood pulp mills. *Nyt Mag Naturvidenskaberne* 1932;71.
- [2] Roose-Amsaleg C, Brygoo Y, Harry M. Ascomycete diversity in soil-feeding termite nests and soils from a tropical rainforest. *Environ Microbiol* 2004;6:462–9. <https://doi.org/10.1111/j.1462-2920.2004.00579.x>.
- [3] Barron GL. New Species and New Records of *Oidiodendron*. *Can J Bot* 1962;40:589–607. <https://doi.org/10.1139/b62-055>.
- [4] Morrall RAA. Two new species of *Oidiodendron* from boreal forest soils. *Can J Bot* 1968;46:203–6. <https://doi.org/10.1139/b68-034>.
- [5] Calduch M, Gené J, Cano J, Stchigel AM, Guarro J. Three new species of *Oidiodendron* Robak from Spain. vol. 50. 2004.
- [6] Rice A V., Currah RS. *Oidiodendron*: A survey of the named species and related anamorphs of *Myxotrichum*. *Stud Mycol* 2005;53:83–120. <https://doi.org/10.3114/sim.53.1.83>.
- [7] COUTURE M, FORTIN JA, DALPE Y. *Oidiodendron* Griseum Robak: an Endophyte of Ericoid Mycorrhiza in *Vaccinium* Spp. *New Phytol* 1983;95:375–80. <https://doi.org/10.1111/j.1469-8137.1983.tb03505.x>.
- [8] Martino E, Perotto S, Parsons R, Gadd GM. Solubilization of insoluble inorganic zinc compounds by ericoid mycorrhizal fungi derived from heavy metal polluted sites. vol. 35. 2003. [https://doi.org/10.1016/S0038-0717\(02\)00247-X](https://doi.org/10.1016/S0038-0717(02)00247-X).
- [9] De Tommaso G, Salvatore MM, Nicoletti R, DellaGreca M, Vinale F, Bottiglieri A, et al. Bivalent metal-chelating properties of harzianic acid produced by *Trichoderma pleuroticola* associated to the gastropod *Melarhaphe neritoides*. *Molecules* 2020;25. <https://doi.org/10.3390/molecules25092147>.
- [10] Bennett JW, Bentley R. What's in a Name?-Microbial Secondary Metabolism. *Adv Appl Microbiol* 1989;34:1–28. [https://doi.org/10.1016/S0065-2164\(08\)70316-2](https://doi.org/10.1016/S0065-2164(08)70316-2).
- [11] Vinale F, Manganiello G, Nigro M, Mazzei P, Piccolo A, Pascale A, et al. A novel fungal metabolite with beneficial properties for agricultural applications. *Molecules* 2014;19:9760–72. <https://doi.org/10.3390/molecules19079760>.
- [12] Keller NP. Fungal secondary metabolism: regulation, function and drug discovery. *Nat Rev Microbiol* 2019;17:167–80. <https://doi.org/10.1038/s41579-018-0121-1>.
- [13] Hambleton S, Egger KN, Currah RS. The genus *Oidiodendron*: species delimitation and phylogenetic relationships based on nuclear ribosomal DNA analysis. *Mycologia* 1998;90:854–68. <https://doi.org/10.1080/00275514.1998.12026979>.
- [14] Sawa R, Mori Y, Iinuma H, Naganawa H, Hamada M, Yoshida S, et al. Harzianic acid, a new antimicrobial antibiotic from a fungus. *J Antibiot (Tokyo)* 1994;47:731–2. <https://doi.org/10.7164/antibiotics.47.731>.
- [15] Vinale F, Flematti G, Sivasithamparam K, Lorito M, Marra R, Skelton BW, et al. Harzianic acid, an antifungal and plant growth promoting metabolite from *Trichoderma harzianum*. *J Nat Prod* 2009;72:2032–5. <https://doi.org/10.1021/np900548p>.
- [16] Kunst F, Ogasawara N, Moszer I, Albertini AM, Alloni G, Azevedo V, et al. The complete genome sequence of the gram-positive bacterium *Bacillus subtilis*. *Nature* 1997;390:249–56. <https://doi.org/10.1038/390249a>.

- org/10.1038/36786.
- [17] Zgoda JR, Porter JR. A convenient microdilution method for screening natural products against bacteria and fungi. *Pharm Biol* 2001;39:221–5. <https://doi.org/10.1076/phbi.39.3.221.5934>.
- [18] Müller A, Wenzel M, Strahl H, Grein F, Saaki TNV, Kohl B, et al. Daptomycin inhibits cell envelope synthesis by interfering with fluid membrane microdomains. *Proc Natl Acad Sci U S A* 2016;113:E7077–86. <https://doi.org/10.1073/pnas.1611173113>.
- [19] Schindelin J, Arganda-Carreras I, Frise E, Kaynig V, Longair M, Pietzsch T, et al. Fiji: An open-source platform for biological-image analysis. *Nat Methods* 2012;9:676–82. <https://doi.org/10.1038/nmeth.2019>.
- [20] Lamsa A, Liu WT, Dorrestein PC, Pogliano K. The *Bacillus subtilis* cannibalism toxin SDP collapses the proton motive force and induces autolysis. *Mol Microbiol* 2012;84:486–500. <https://doi.org/10.1111/j.1365-2958.2012.08038.x>.
- [21] Chen JL, Steele TWJ, Stuckey DC. Modeling and Application of a Rapid Fluorescence-Based Assay for Biototoxicity in Anaerobic Digestion. *Environ Sci Technol* 2015;49:13463–71. <https://doi.org/10.1021/acs.est.5b03050>.
- [22] Kepplinger B, Morton-Laing S, Seistrup KH, Marrs ECL, Hopkins AP, Perry JD, et al. Mode of Action and Heterologous Expression of the Natural Product Antibiotic Vancoresmycin. *ACS Chem Biol* 2018;13:207–14. <https://doi.org/10.1021/acscchembio.7b00733>.
- [23] Thakur S, Cattoni DI, Nöllmann M. The fluorescence properties and binding mechanism of SYTOX green, a bright, low photo-damage DNA intercalating agent. *Eur Biophys J* 2015;44:337–48. <https://doi.org/10.1007/s00249-015-1027-8>.
- [24] Kleijn LHJ, Oppedijk SF, T Hart P, Van Harten RM, Martin-Visscher LA, Kemmink J, et al. Total Synthesis of Laspartomycin C and Characterization of Its Antibacterial Mechanism of Action. *J Med Chem* 2016;59:3569–74. <https://doi.org/10.1021/acs.jmedchem.6b00219>.
- [25] van der Beek SL, Le Breton Y, Ferenbach AT, Chapman RN, van Aalten DMF, Navratilova I, et al. GacA is essential for Group A *Streptococcus* and defines a new class of monomeric dTDP-4-dehydrorhamnose reductases (RmlD). *Mol Microbiol* 2015;98:946–62. <https://doi.org/10.1111/mmi.13169>.
- [26] Schaub R, Dillard J. Digestion of Peptidoglycan and Analysis of Soluble Fragments. *Bio-Protocol* 2017;7. <https://doi.org/10.21769/bioprotoc.2438>.
- [27] Smith TJ, Foster SJ. Characterization of the involvement of two compensatory autolysins in mother cell lysis during sporulation of *Bacillus subtilis* 168. vol. 177. 1995. <https://doi.org/10.1128/jb.177.13.3855-3862.1995>.
- [28] Kasianowicz J, Benz R, McLaughlin S. The kinetic mechanism by which CCCP (carbonyl cyanide *m*-Chlorophenylhydrazone) transports protons across membranes. *J Membr Biol* 1984;82:179–90. <https://doi.org/10.1007/BF01868942>.
- [29] Prince A, Sandhu P, Kumar P, Dash E, Sharma S, Arakha M, et al. Lipid-II Independent Antimicrobial Mechanism of Nisin Depends on Its Crowding and Degree of Oligomerization. *Sci Rep* 2016;6:1–15. <https://doi.org/10.1038/srep37908>.
- [30] Boger DL. Vancomycin, teicoplanin, and ramoplanin: Synthetic and mechanistic studies. *Med Res Rev* 2001;21:356–81. <https://doi.org/10.1002/med.1014>.
- [31] Frindert J, Kahloon MA, Zhang Y, Ahmed YL, Sinning I, Jäschke A. YvcI from *Bacillus subtilis* has in vitro RNA pyrophosphohydrolase activity. *J Biol Chem* 2019;294:19967–77. <https://doi.org/10.1074/jbc.119.019967>.

- org/10.1074/jbc.RA119.011485.
- [32] Walker JE. The ATP synthase: The understood, the uncertain and the unknown. *Biochem Soc Trans* 2013;41:1–16. <https://doi.org/10.1042/BST20110773>.
- [33] Kim JY, Inaoka T, Hirooka K, Matsuoka H, Murata M, Ohki R, et al. Identification and characterization of a novel multidrug resistance operon, mdtRP (yusOP), of *Bacillus subtilis*. *J Bacteriol* 2009;191:3273–81. <https://doi.org/10.1128/JB.00151-09>.
- [34] Chan JM, Guttenplan SB, Kearns DB. Defects in the flagellar motor increase synthesis of poly- γ -glutamate in *Bacillus subtilis*. *J Bacteriol* 2014;196:740–53. <https://doi.org/10.1128/JB.01217-13>.
- [35] Russell AD. Whither triclosan? *J Antimicrob Chemother* 2004;53:693–5. <https://doi.org/10.1093/jac/dkh171>.
- [36] Kohanski MA, Dwyer DJ, Wierzbowski J, Cottarel G, Collins JJ. Mistranslation of Membrane Proteins and Two-Component System Activation Trigger Antibiotic-Mediated Cell Death. *Cell* 2008;135:679–90. <https://doi.org/10.1016/j.cell.2008.09.038>.
- [37] Davis BD, Chen L, Tai PC. Misread protein creates membrane channels: An essential step in the bactericidal action of aminoglycosides. *Proc Natl Acad Sci U S A* 1986;83:6164–8. <https://doi.org/10.1073/pnas.83.16.6164>.
- [38] Tieleman DP, Leontiadou H, Mark AE, Marrink SJ. Simulation of pore formation in lipid bilayers by mechanical stress and electric fields. *J Am Chem Soc* 2003;125:6382–3. <https://doi.org/10.1021/ja029504i>.
- [39] Tilley SJ, Saibil HR. The mechanism of pore formation by bacterial toxins. *Curr Opin Struct Biol* 2006;16:230–6. <https://doi.org/10.1016/j.sbi.2006.03.008>.
- [40] Pontes MH, Groisman EA. Slow growth determines nonheritable antibiotic resistance in *Salmonella enterica*. *Sci Signal* 2019;12:3938. <https://doi.org/10.1126/scisignal.aax3938>.
- [41] Berka RM, Hahn J, Albano M, Draskovic I, Persuh M, Cui X, et al. Microarray analysis of the *Bacillus subtilis* K-state: Genome-wide expression changes dependent on ComK. vol. 43. John Wiley & Sons, Ltd; 2002. <https://doi.org/10.1046/j.1365-2958.2002.02833.x>.
- [42] Susanna KA, Fusetti F, Thunnissen AMWH, Hamoen LW, Kuipers OP. Functional analysis of the competence transcription factor ComK of *Bacillus subtilis* by characterization of truncation variants. *Microbiology* 2006;152:473–83. <https://doi.org/10.1099/mic.0.28357-0>.

SUPPORTING INFORMATION

Table S1. HA MIC on pathogenic bacteria. MICs of HA on different pathogenic bacteria were tested starting at a 400 µg/mL which was then serially diluted with a factor 2. a = Gift from University Medical Center Utrecht; b = ATCC strains.

Strain	Gram	MIC (µg/mL)
<i>Acinetobacter baumannii</i> 1179 ^a	-	> 400
<i>Acinetobacter nosocomialis</i> 14-8211 ^a	-	> 400
<i>Enterobacter cloacae</i> complex MC04842 ^a	-	> 400
<i>Escherichia coli</i> TEM-3 GVJS004 ^a	-	> 400
<i>Klebsiella pneumoniae</i> SHV-18 GVJS006 ^a	-	> 400
<i>Pseudomonas aeruginosa</i> ATCC57853 ^b	-	> 400
<i>Stenotrophomonas maltophilia</i> GV20A226 ^a	-	> 400
<i>Enterococcus faecium</i> VRE GV16D030 ^a	+	100
<i>Enterococcus faecium</i> GV15A623 ^a	+	50
<i>Listeria monocytogenes</i> GV21-4a ^a	+	25
<i>Staphylococcus aureus</i> MSSA 476 GVS0101 ^a	+	50
<i>Staphylococcus aureus</i> MRSA USA300 GVS1474 ^a	+	200
<i>Staphylococcus epidermidis</i> GV08A1071 ^a	+	50
<i>Streptococcus pneumoniae</i> 05A396 ^a	+	25

Table S2. Exogenous Lipid II and its precursors did not affect HA antimicrobial activity.

Vancomycin, nisin and HA have an antimicrobial effect on *B. subtilis*. Quenching of this antimicrobial effect was tested by addition of exogenous Lipid II and precursors (10 µM for nisin and vancomycin and either 10 µM or 150 µM for HA; results of both lipid concentrations on antimicrobial effect of HA were similar) prior to the addition of indicated antimicrobials at 1 × or 2 × their MIC as indicated. Bacterial growth was assessed and the assay scored as unaffected (-) or affected (+) by the addition of exogenous lipid.

Antagonist	Vancomycin (2 × MIC)	Nisin (2 × MIC)	HA (2 × MIC)	HA (1 × MIC)
Blank	-	-	-	-
Lipid I	+	+	-	-
Lipid II	+	+	-	-
C55-P	-	+	-	-

Table S3. *B. subtilis* strain M9015 harbors five mutations in four genes. Bioinformatic analysis of the genome sequences of *B. subtilis* strain 168 and M9015 results in 10 possible mutations, five of which are reliable. The position of the mutations is indicated and is based on the reference genome NC_000964.3. The mutations were visualized using Integrated Genomics Viewer and the gene names of the verified reliable mutations are indicated.

# Mutation	Position	WT	M9015	Reliable?	Mutated gene
1	353056	AAGCAGCTGATC GAGCAGCTGA	AAGCAGCTGA	No	/
2	1872540	T	C	Yes	<i>ymaB</i>
3	2152047	A	C	No	/
4	2480653	CT	C	No	/
5	2480666	GT	G	No	/
6	2581726	GTTTTTT	GTTTTTT	No	/
7	3374690	G	GA	Yes	<i>yusO</i>
8	3374945	AGAGGAAACGGA	AGAGGAAACGGAGGAAACGGA	Yes	<i>yusO</i>
9	3638128	ATTTTTTTT	ATTTTTTTT	Yes	<i>figL</i>
10	3786681	G	A	Yes	<i>atpE</i>

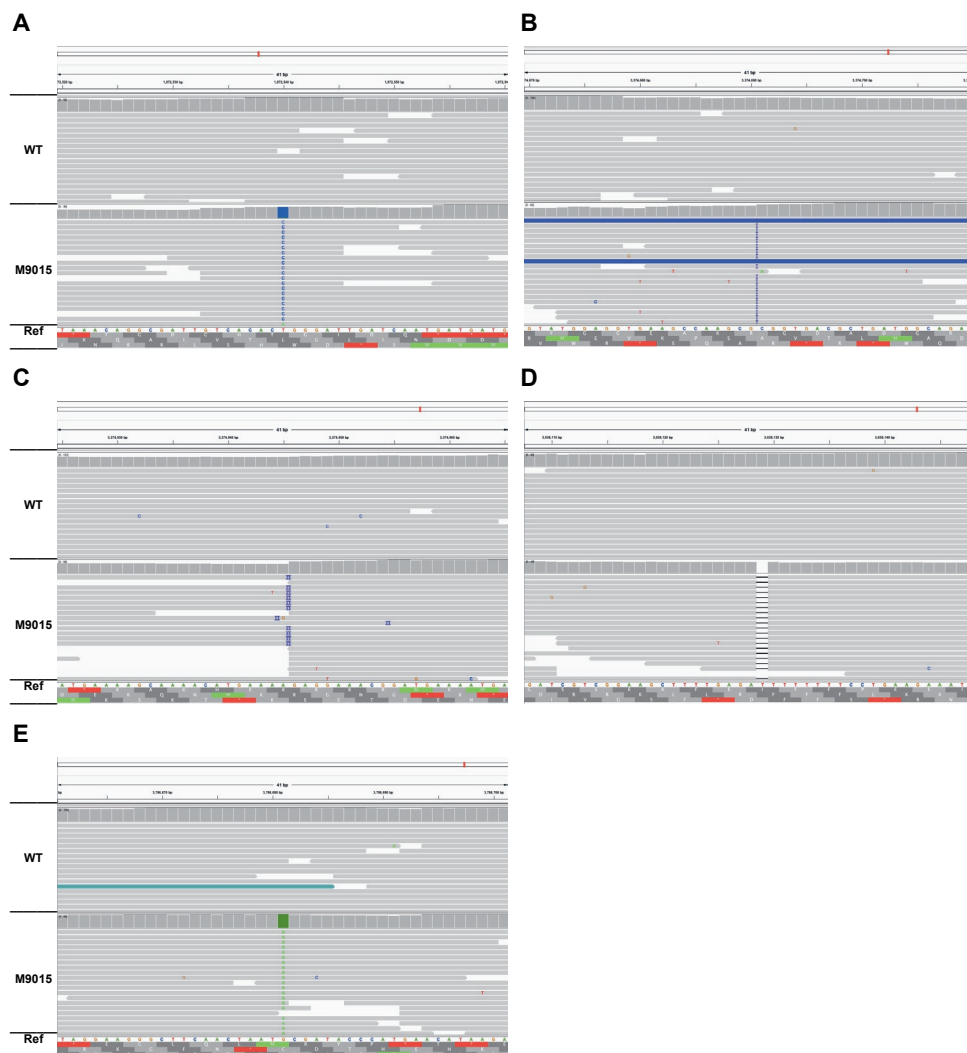


Fig. S1. Viewing gene variations with Integrated Genomics Viewer (I). 10 predicted mutated sites were verified using Integrated Genomics Viewer. Five correctly predicted mutations (Mutation#2, #7-#10) (see Table 2) were listed in (A) to (E). “Ref” indicated the reference genome. Representative reads (around 15) were presented for both WT and M9015.

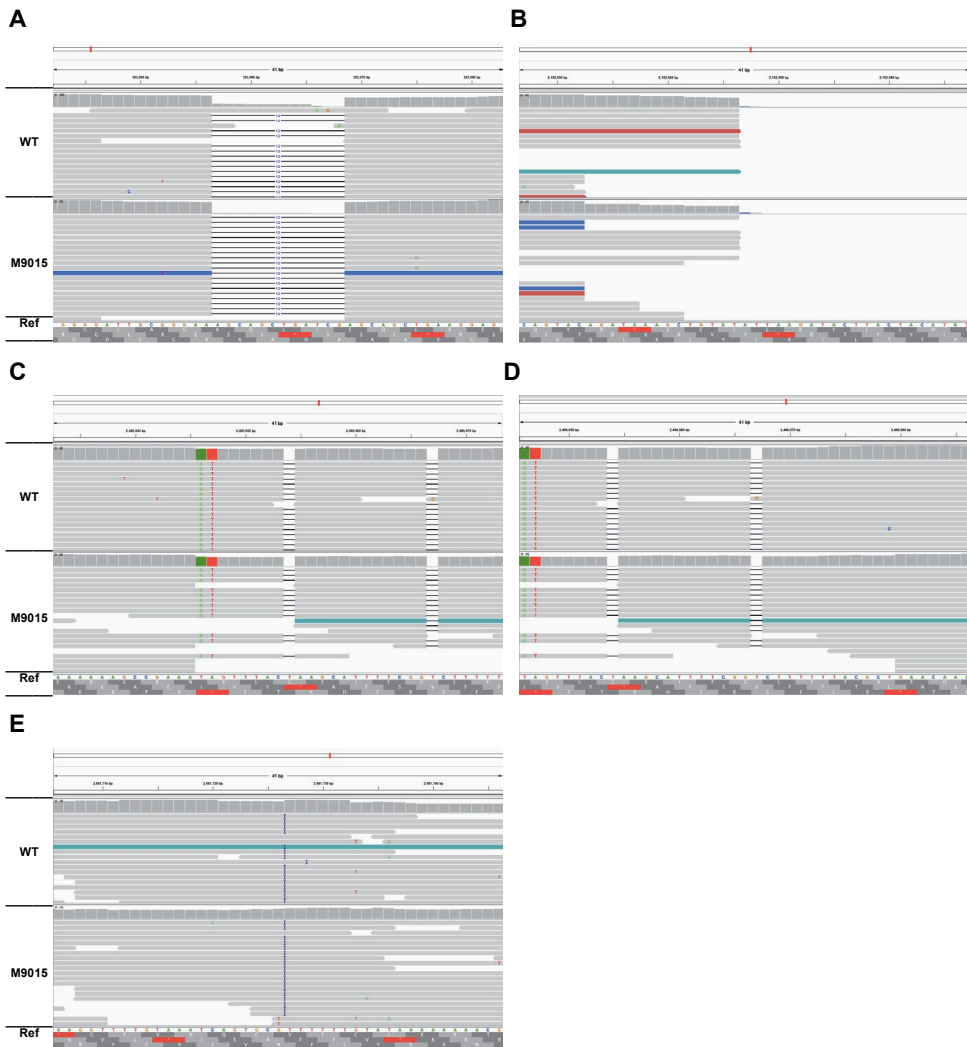


Fig. S2. Viewing gene variations with Integrated Genomics Viewer (II). 10 predicted mutated sites were verified using Integrated Genomics Viewer. Five wrongly predicted mutations (Mutation#1, #3-#6) (see Table 2) were listed in (A) to (E). “Ref” indicated the reference genome. Representative reads (around 15) were presented for both WT and M9015.

